Performance of EGNSS-based Timing in Various Threat Conditions.

Performance of EGNSS-based Timing in Various Threat Conditions

Salomon Honkala, Sarang Thombre, Martti Kirkko-Jaakkola, Hein Zelle, Henk Veerman, Anders E. Wallin, Erik F. Dierikx, Sanna Kaasalainen, Stefan Söderholm, Heidi Kuusniemi

***Abstract*—Today's society is highly reliant on time and frequency synchronization, for example in communications systems and financial networks. Precise timing is more and more derived from satellite navigation receivers, which are unfortunately very susceptible to various signal threats. We studied the performance of Global Navigation Satellite System (GNSS) timing under different operating conditions, and tested the effectiveness of different techniques that improve timing receiver robustness. These features were tested under various threat scenarios related to specific vulnerabilities in GNSS-based timing, such as interference and navigation message errors, and their efficiency was analyzed against corresponding scenarios. We found that interference or meaconing-type spoofing can threaten GNSS timing, but can be detected by means of automatic gain control (AGC) and carrier-to-noise ratio based methods. GNSS interruptions due to interference can be bridged by a local oscillator holdover technique based on a Kalman filter whose parameters are based on a GNSS time solution. Navigation message errors are mitigated by the European Geostationary Navigation Overlay Service (EGNOS), and constellation-wide timing errors can be detected by the use of a dual-constellation (GPS-Galileo) cross-check. Dual-frequency operation for timing, in addition to mitigating first-order ionospheric effects, was found to be more robust to interference with the option to fall back to single frequency.**

***Index Terms*—Global navigation satellite system; Global Positioning System; Time dissemination; Robustness.**

I. Introduction

TIME and frequency synchronization is a vital dependency in critical infrastructures such as telecommunication networks and power grids. Many users of precise timing have adopted the Global Navigation Satellite Systems (GNSS), such as Global Positioning System (GPS), as a globally available source of primary time reference.

When GNSS is used for navigation it relies on the atomic clocks on board the satellites for accurate time measurements, which are in turn used to make range measurements to the satellites. As a side effect of positioning, the receiver clock is synchronized with the GNSS time. In effect, GNSS can be used as a time transfer system, and provides timing with an accuracy of some tens of nanoseconds [1]–[4].

Each GNSS has its own system time. GNSS time scales are kept synchronized with Coordinated Universal Time (UTC), typically to the nanosecond level. The estimated offset between GNSS time and UTC is included in the navigation signals, so a receiver can obtain an estimate of both GNSS time and UTC.

However, GNSS signals received on the Earth are extremely weak in power, rendering them susceptible to interference which can be either unintentional, such as side-band interference from other transmitters, or intentional GNSS jammers. A spoofing attack, by the transmission of counterfeit GNSS signals, against timing is seen as a significant threat [5]–[7], and various countermeasures have been investigated [8]–[10]. Furthermore, natural effects, such as signal reflections and atmospheric propagation, i.e., ionospheric disturbances and tropospheric refraction, can cause increased errors.

Other vulnerabilities exist in the GNSS system in total, which consists of many interconnected parts, where various failure scenarios can lead to an interruption or fault in the signal. A fault may affect a single satellite (e.g. a clock malfunction or a faulty orbit prediction) or all satellites of a constellation (e.g. a faulty navigation message upload). While these failures are extremely rare as robust safeguards and redundancies are built into the systems, they have occurred in the past, such as in 2016, when the GPS UTC offset parameter was erroneous, causing disturbances in timing systems [11]. Such incidents and the general need to maintain continuity of precise timing services has led to ongoing studies on utilizing terrestrial positioning, navigation, and timing (PNT) systems, e.g. Enhanced Long Range Navigation (eLORAN) [12] and DGNSS Ranging Mode (R-MODE) [13], as robust back-up options.

Previous work has studied GPS/GNSS timing focusing on accuracy in timing synchronization [1], [14]–[19], high precision time transfer for primary standards and metrology laboratories [3], [4], [20]–[22], and the use of new constellations such as Galileo [23], [24]. Receiver features to enhance robustness have been investigated, ranging from directional antennas and alternative signal sources [25] to Receiver Autonomous Integrity Monitoring (RAIM) applied to timing, i.e., T-RAIM [1]. In addition, the European Geostationary Navigation Overlay Service (EGNOS) transmits augmentation data to improve accuracy and integrity of GPS navigation

This research was conducted within the project "Advanced Mission Concepts: R&D for Robust EGNSS Timing Services" funded by the Directorate-General for Internal Market, Industry, Entrepreneurship and SMEs (DG-GROW) of the European Commission. *Corresponding authors: S. Honkala; S. Thombre*

S. Honkala, S. Thombre, M. Kirkko-Jaakkola, and S. Kaasalainen are with the Finnish Geospatial Research Institute, Kirkkonummi, Finland. (e-mail: salomon.honkala@nls.fi; sarang.thombre@nls.fi)

H. Kuusniemi is with the Finnish Geospatial Research Institute, and also with the University of Vaasa, Finland.

S. Söderholm is with HERE Technologies, Tampere, Finland, and also with the Finnish Geospatial Research Institute.

H. Zelle and H. Veerman are with the Netherlands Aerospace Center NLR, Marknesse, The Netherlands.

A. E. Wallin is with VTT Technical Research Centre of Finland Ltd, Centre for Metrology MIKES, Espoo, Finland

E. F. Dierikx is with VSL, Delft, The Netherlands.

within Europe [26]. This augmentation can also be applied to GNSS timing.

In the scope of this work, we assessed the use of the European GNSS (EGNSS) services, Galileo [27] and EGNOS, for time determination and their performance in different threat conditions. The newly developed multi-GNSS software-defined receiver FGI-GSRx [28] is used in computing the timing solutions based on raw GNSS data and enables a level of detail in analyzing the performance and robustness that has not been possible previously. We focus on the robustness of the services, since the timing community is mostly concerned about the availability and resilience of timing, while accuracy requirements of most users are easily met by GNSS [29].

This paper builds upon our previous work in [30], where the key performance indicators (KPIs) were first defined, the test setup was introduced and used to evaluate Galileo and EGNOS timing robustness and demonstrate the effectiveness of T-RAIM with Galileo. In [31], initial results on jamming detection, T-RAIM, and dual-constellation cross-check were published.

Our present results further evaluate the performance of the time determination under different operating conditions, such as ionospheric disturbance and spoofing, and demonstrate the effectiveness of different techniques that improve timing receiver robustness, including GNSS Disciplined Oscillator (GNSSDO) holdover.

The remainder of this paper is organized as follows: Section II provides a general overview of the GNSS timing services and the robustness techniques. Section III describes the KPIs selected for performance evaluation, and Section IV introduces the experimental methods adopted for timing robustness evaluation and improvement. The experimental results are provided in Section V. Conclusions are drawn in Section VI.

II. Overview of GNSS Timing

Specialized GNSS timing receivers are nearly identical to navigation receivers, but their primary outputs are 1 pulse-per-second (1PPS) and 10 MHz frequency signals. Typical use of GNSS for timing is as part of a GNSS disciplined oscillator (GNSSDO), which is a cost-effective piece of equipment that provides an accurate timing reference [32].

We consider the use of GNSS for timing as a part of a GNSSDO having a local oscillator (LO), e.g., a temperature-compensated crystal (TCXO), oven-controlled crystal (OCXO), or rubidium oscillator. A GNSS receiver provides accurate time, and the oscillator is steered towards the GNSS time. The disciplined oscillator provides a frequency and 1PPS output, synchronized to GNSS time. A GNSSDO is usually stationary, and can take advantage of the known static position for better accuracy and robustness in the computation of a GNSS time solution.

The GNSS receiver may experience interruptions in the signal due to interference or blockage of the antenna. In this situation the GNSSDO will continue to operate in holdover mode, based only on its internal oscillator. The clock will begin to drift, however the disciplining loop will implement a holdover function based on the oscillator model generated while GNSS was available.

GNSS receivers normally have an automatic gain control (AGC) block, which controls the incoming power level at the radio front-end. The individual received signal strengths of the signals are measured by carrier–to–noise density ratio C/N_0.

In this article we analyze several techniques to study and improve the EGNSS-based timing performance of a commercial receiver driven by an external TCXO reference. These techniques are broadly based on:

- Multi-constellation (GPS-Galileo) GNSS
- Multi-frequency GNSS
- EGNOS augmentation
- Interference and spoofing detection
- Local oscillator holdover

III. Key Performance Indicators for Robust Timing

This section presents the metrics we used as the key performance indicators in evaluating the GNSS timing solutions and the robustness features. These performance metrics are evaluated in light of the International Telecommunication Union (ITU) recommendation on Primary Reference Time Clock (PRTC) characteristics [33]. This scenario was chosen as the benchmark as the recommendations are well defined and telecommunications is one of the most common use cases for GNSS-based timing.

A. Accuracy

We evaluate the accuracy of the timing solution by comparing both the time (phase) offset and the frequency offset of the timing receiver to a reference clock.

The absolute accuracy of the time signal is measured by the time offset and the frequency offset [34]. Time offset is defined as the difference between a measured on-time pulse and a reference on-time pulse expressed as:

$$\Delta t_i = t_{meas}(i) - t_{ref}(i), \tag{1}$$

where i is the index of the measurement epoch. Frequency offset is the offset of the measured frequency from the nominal frequency, defined as

$$\delta f = \frac{f_{meas} - f_{ref}}{f_{ref}}, \tag{2}$$

and expressed as a dimensionless number, often as parts per million (ppm).

B. Stability

Stability measures the changes in frequency over certain periods of time. Various stability metrics exist, but we consider the maximum time interval error (MTIE) and the time deviation (TDEV). MTIE measures the worst-case time error, while TDEV describes the noise properties of the clock.

MTIE refers to the largest variation of the time offset $\Delta t_i,\ i = 1, 2, \ldots, N$ within an analysis interval τ, expressed as [34]

$$\mathrm{MTIE}(\tau) = \max_{1 \le k \le N-n} \left(\max_{k \le i \le k+n} \Delta t_i - \min_{k \le i \le k+n} \Delta t_i \right) \tag{3}$$

TABLE I
ITU PRTC LIMITS FOR MTIE AS A FUNCTION OF ANALYSIS INTERVAL τ.

$0.275 \times 10^{-3}\tau + 0.025$ µs	for	$0.1 < \tau \leq 1000$ s
$10^{-5}\tau + 0.29$ µs	for	$\tau > 1000$ s

TABLE II
ITU PRTC LIMITS FOR TDEV AS A FUNCTION OF ANALYSIS INTERVAL τ.

3 ns	for	$0.1 < \tau \leq 100$ s
0.03 τ ns	for	$100 < \tau \leq 1000$ s
30 ns	for	$1000 < \tau < 10\,000$ s

where the integer $n = 1, 2, \ldots, N-1$ is the number of measurements within a particular analysis interval τ, N is the total number of time offset measurements, and $\tau = n\tau_0$, where the sampling time is τ_0.

TDEV is a measure of time stability computed from (M+1) time offset measurements $\Delta t_i, i = 1, 2, \ldots, M+1$, for analysis interval τ as

$$\mathrm{TDEV}(\tau) = \frac{\sqrt{\sum_{j=1}^{M-3m+2}\left(\sum_{i=j}^{j+m-1}(\Delta t_{i+2m} - 2\Delta t_{i+m} + \Delta t_i)\right)^2}}{m\sqrt{6(M-3m+2)}} \quad (4)$$

where the integer m denotes the number of measurements corresponding to the averaging time τ [34].

Specific requirements for these metrics are given by the ITU [33]. The ITU recommendations for MTIE and TDEV are listed in Tables I and II.

IV. Experimental Methods for Evaluating the KPIs

In order to evaluate the KPIs for robust timing, we conducted three data collection phases, each lasting several days. In order to obtain a precise time reference, we used the reference time and frequency generated at the MIKES metrology laboratory, the basis for Finland's UTC time, UTC(MIKE). During the data collection, the offset of the 1PPS signal output by the receiver with respect to UTC(MIKE) was measured.

A. Instrumentation

We collected GNSS data using a roof-mounted GNSS antenna at the national metrology lab MIKES in Espoo, Finland. The receiver data collection configuration is illustrated in Fig. 1. Raw GNSS observations (pseudoranges) and navigation data were logged by a geodetic-type GNSS receiver [35]. The receiver used an external 10 MHz TCXO connected to its 10 MHz frequency input as its LO [36]. A low-cost clock was selected, in order to highlight the effect of GNSS and to present significant errors in a short period of time. UTC(MIKE) was directly used as the reference time in all measurements. A time interval counter (TIC) [37], set up as a frequency counter, logged a time series of the frequency offsets of the LO with respect to a reference frequency FREQ(k) which is phase locked to UTC(MIKE). Another TIC logged

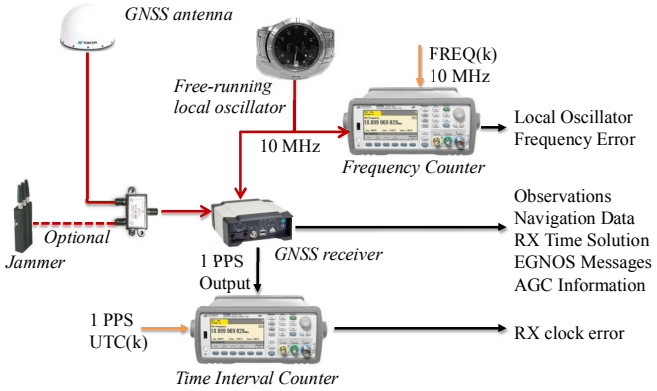

Fig. 1. Test setup for receiver data collection. This setup is used for computing timing stability metrics under different threat scenarios, including jamming.

the offsets between the 1PPS output of the receiver and the reference time.

The logged GNSS data included GNSS observables for all frequencies, broadcast navigation data, EGNOS data, receiver C/N_0, and AGC levels separately for the E1 and E5 frequency bands. The logged observations were processed using FGI-GSRx, a multi-GNSS software receiver [28], which calculated the time solutions. In conjunction with the GNSS processing, a clock controller block estimated the steering corrections necessary for synchronizing the phase and frequency of the LO with the GNSS time, based on the GNSS solution and the intrinsic stability parameters of the LO.

The receiver clock error was determined using the time solution reported by the receiver and the measured offset between the 1PPS output and UTC(MIKE). Then, the GNSS time solution was computed from the observations, their time stamps, and the broadcast GNSS time to UTC model, and calibrated for cable delays.

The difference between the GNSS solution and the measured clock error constituted the time offset Δt that was used to calculate the MTIE and TDEV as described in Sect. III.

As necessary for specific test scenarios, the software applied EGNOS corrections and T-RAIM, and added simulated GNSS data errors, in order to test different receiver configurations and threat scenarios.

B. Threat scenarios

The performance of GNSS timing was investigated under two categories of threat scenarios. Firstly, threats which affect individual satellites, such as errors in the navigation message and multipath. Secondly, threats which produce a multiple-satellite fault, such as elevated ionospheric activity, radio frequency interference due to jamming, and signal spoofing. In each case, initially the time solution was calculated without threats and the time solution error with respect to UTC was estimated. Next, upon introduction of the threat a new time solution was calculated and compared to the original reference solution, thus demonstrating the impact of the threat. The manner of producing the threats and introducing them into the experiments is described below.

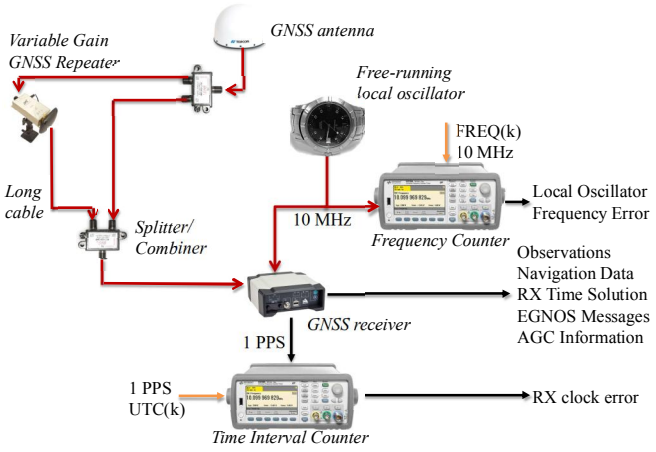

Fig. 2. Test setup for computing timing stability metrics under the spoofing scenario.

Errors in the navigation message: These test cases investigate the effect on GNSS timing of conditions arising from misleading information in a satellite's navigation data or malicious modification of the navigation data from unauthorized sources. In the first test case, to test how such errors affect the time solution, as an arbitrary example the recorded clock bias parameter (a_{f0}) in the navigation data for any one satellite was manually modified for a period of four hours during the test. In the second test case, to simulate a constellation-wide navigation data error or misleading information in the UTC offset parameters, the clock bias parameter of all satellites in one GNSS constellation was modified for a period of four hours during the test.

Multipath: This test case investigates the effect of a non-trivial multipath error affecting the pseudorange measurement from one or two of the visible satellites. The error was introduced manually in the pseudorange measurements recorded by the GNSS receiver. A multipath offset of either 3 m or 10 m was introduced on both frequencies of the Galileo satellite(s).

Ionosphere: This test case investigates the effect on EGNSS timing of elevated ionospheric activity in a part of the atmosphere. Such a scenario would manifest as a distance error in the measured pseudorange of satellites whose line of sight vector passes through the affected part of the ionosphere. The error was computed as a function of the signal frequency and the total electron content units (TECU) for the elevated ionospheric activity, assumed here as 100 TECU. Additionally, a random noise term was included in order to reduce the correlation between the different affected pseudoranges. These errors were introduced by manually altering the measured pseudoranges of three satellites for a period of six hours.

Radio frequency interference (jamming): This test case investigates the effect of radio frequency interference on the receiver observables, such as AGC and C/N_0, and on the timing solution itself. The interference threat was introduced in two ways: First, for validating methods of jamming detection by observing the AGC and C/N_0 behavior of the receiver, short data sets (e.g., 5 minutes each) are sufficient. In this case, actual RF interference from low-cost portable Covert GPS Signal Blockers (chirp-signal jammers) operating either on the L1 frequency or the entire L-band was mixed into the RF cable before the GNSS receiver, as shown in Fig. 1. Periods of interference were alternated with periods of no interference, and the jammer to signal ratio was progressively increased from about 10 dB to about 95 dB. Second, the effect of interference on the time solution requires evaluation based on 24-hour recorded data sets. The interference was then simulated by introducing artificial gaps in the recorded data representing complete loss of GNSS signals during a hypothetical jamming incident.

Signal spoofing: This test case investigates the effect of meaconing-type signal spoofing, i.e. introducing exactly the same signals as the original but with a time delay, in order to confuse the GNSS receiver and interfere with its normal operation. The test setup is illustrated in Fig. 2. The threat from spoofing was introduced by extracting the original signal through a radio frequency splitter and introducing it again into the signal stream after some delay. This was in turn achieved by passing the spoofing signal through a very long cable of length up to a few tens of meters. The spoofing signal to actual signal time delay was approximately 100 ns. Before the long cable, the GNSS signals were amplified with the help of an adjustable-gain GNSS signal repeater. The ratio of the spoofing power to the original signal was –20 dB at minimum, and +14 dB at maximum, achieved by varying the repeater gain setting and accounting for cable attenuation. The overall test duration was about 38 min.

V. Experimental Results

We used the data collected by the procedures described in Section IV to test the various threats and robustness methods. This section presents the results of these tests.

A. Baseline Test

First, tests were carried out to verify the performance of GPS, Galileo, and EGNOS based timing with respect to the performance metrics presented in Sect. III, when no threats are present. These tests were conducted in order to verify that the test setup complies with the performance requirements for GNSS-based timing [33] under nominal operating conditions. This test serves as the baseline for the other tests, where we evaluated the timing performance in presence of the threats described in Sect. IV.

The tested GNSS configurations included single-frequency (SF) GPS (between 7 and 14 satellites used in the timing solution), SF GPS–EGNOS (7-13 satellites), dual-frequency (DF) GPS (L1-L5) (3-7 satellites), SF Galileo (E1) (3-7 satellites), and DF Galileo (E1-E5a) (3-7 satellites). Their MTIE and TDEV were determined over a data series of 24 hours starting from 00:00:00 to 23:59:59 on 20 April, 2017.

Fig. 3 compares the MTIE in the baseline GNSS solutions to the ITU recommendation for maximum MTIE. The MTIE for the free-running LO without GNSS is not shown in Fig. 3, as it would be out of range due to its frequency offset and therefore cannot provide an absolute time reference that would satisfy the recommendation. The measured normalized

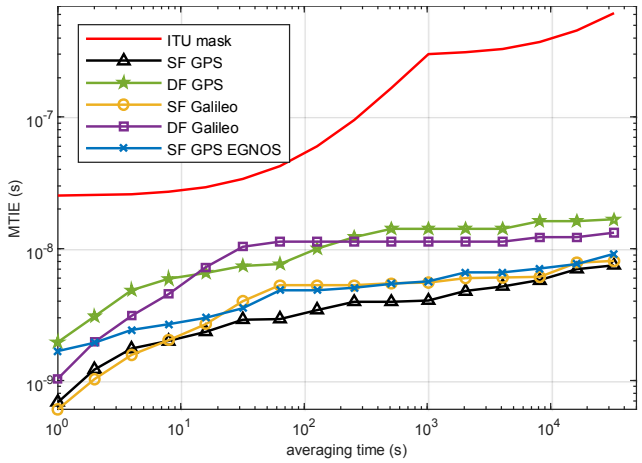

Fig. 3. Comparison based on MTIE shows that baseline GNSS timing solutions satisfy the ITU recommendation for a PRTC.

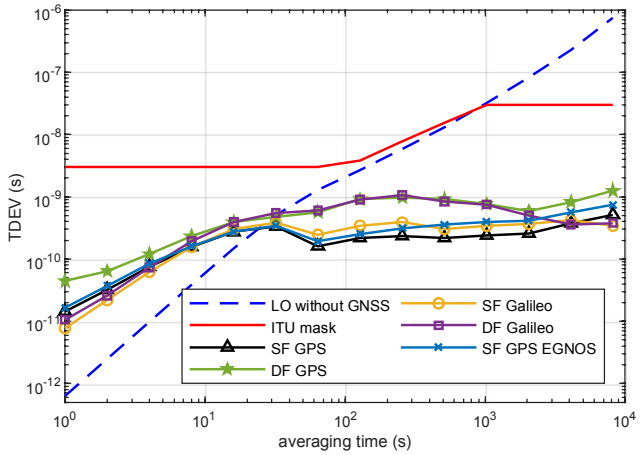

Fig. 4. Comparison based on TDEV also shows that baseline GNSS timing solutions satisfy the ITU recommendation for a PRTC.

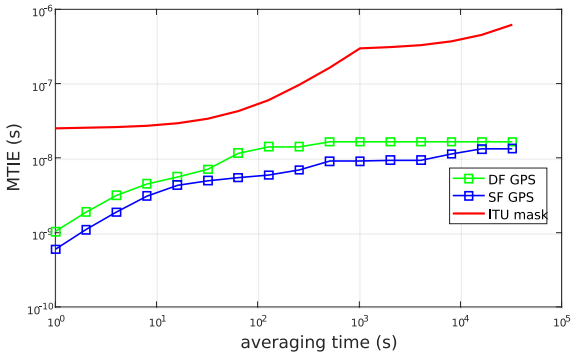

Fig. 5. Comparison based on MTIE between DF GPS and SF GPS by simulating the timing solution using same number of satellites.

frequency offset of the LO ranged from -0.177 to -0.179 ppm. The figure asserts that the MTIE of the GNSS-based timing solutions remain within the ITU recommendation.

Fig. 4 compares the TDEV for the GNSS timing solutions and the free-running LO to the ITU recommendation. It is noted that the free-running LO partly achieves the ITU

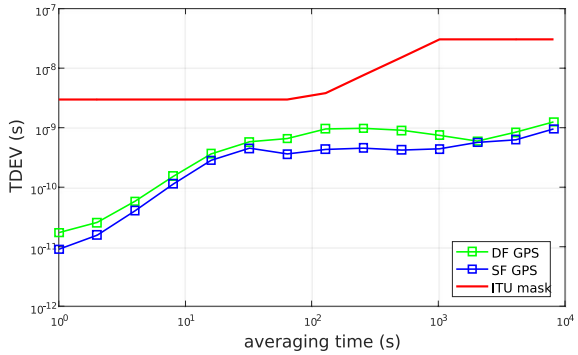

Fig. 6. Comparison based on TDEV between DF GPS and SF GPS by simulating the timing solution using same number of satellites.

recommendation for TDEV at short averaging times, but the GNSS solution brings the long-term stability fully within the recommended levels.

The DF GPS configuration shows an elevated MTIE compared to SF, which can be explained partly by the lower number of satellites used (between 2-6 in DF as compared to between 7-14 in SF), since only some of the GPS satellites transmit the L5 signals. Another cause is the additional noise resulting from the combination of the dual-frequency observables. The TDEV results are also higher than in the single-frequency GPS configuration. To validate the performance under more fair conditions, the MTIE and TDEV were computed for SF and DF GPS by simulating the timing solution using same number of satellites (between 2-6). Figs. 5 and 6 compare the performance of SF and DF GPS under this hypothetical scenario. It can be observed that in spite of same number of satellites, the MTIE and TDEV are elevated for the DF case. Returning to Figs. 3 and 4, similar to the DF GPS case, the DF Galileo configuration shows an elevated MTIE and TDEV compared to SF.

The SF GPS–EGNOS has slightly higher MTIE and TDEV than SF GPS only, mainly because the EGNOS solution used fewer satellites than the GPS-only solution. Note that the data was collected in Southern Finland, close to the northeastern edge of the EGNOS coverage area, and therefore some GPS satellites that are visible, being outside the area, are not monitored by EGNOS and are therefore excluded.

The Galileo SF results are similar to the single-frequency GPS configuration, and similar conclusions can be drawn. Note that the number of active Galileo satellites increased by two in May 2017, after the previous data was collected. In a subsequent repeat of this test, the number of Galileo satellites available for the timing solution had increased, and a slight improvement in Galileo MTIE and TDEV was seen at shorter averaging times. Consequently, as a further comparison between the GPS and Galileo solutions, considering that GPS has almost twice the number of satellites used in the timing solution, we compared the two constellations in the hypothetical situation where the number of satellites is similar for both constellations. The number of GPS satellites included in the solution was reduced to that of Galileo (varying between 3 and 7), while maintaining a comparable C/N_0 distribution.

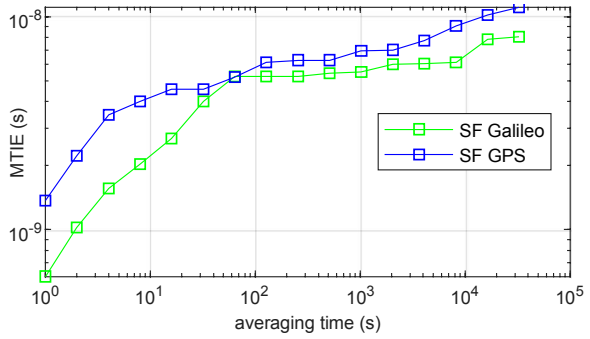

Fig. 7. Comparison of MTIE for single-frequency Galileo and GPS in a hypothetical scenario of equal number of satellites used for GPS and Galileo.

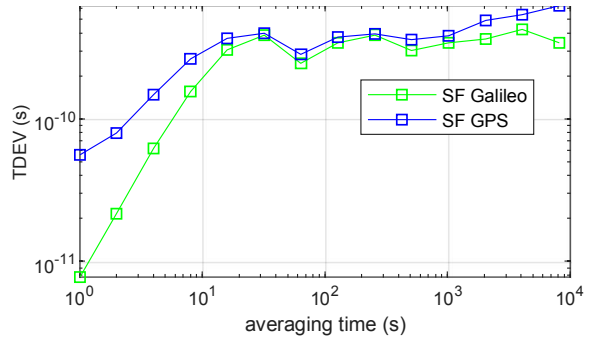

Fig. 8. Comparison of TDEV for single-frequency Galileo and GPS in a hypothetical scenario of equal number of satellites used for GPS and Galileo.

Figures 7 and 8 show the MTIE and TDEV results of this test, which imply that the performance of Galileo is equivalent or slightly better than the GPS-based solution.

Overall, these test results verify that GNSS-based timing satisfies the ITU recommendation in all of the receiver configurations. Next, these tests were used as a baseline when evaluating the timing performance in the presence of threats described in Sect. IV, and the effectiveness of the proposed countermeasures.

B. Errors in the navigation message

The effect of misleading information in a satellite's navigation data was studied using a simulated data error. In accordance with the service-level definition of EGNOS it is assumed that the data error triggers a simulated EGNOS message flagging the affected satellites as unsafe. As a result the timing solution no longer uses the unsafe satellites. Fig. 9 shows the time offset of the GPS and GPS–EGNOS solution during the simulated fault. The GPS solution is adversely affected, while the EGNOS solution maintains nominal behavior and successfully excludes the error. Note that currently, EGNOS can only be used in combination with GPS, as EGNOS V3 that will support Galileo is not yet available.

The use of multi-constellation GNSS in the mitigation of a constellation-wide navigation data fault was also examined. A dual-constellation cross-check is used so that a single constellation-wide fault can be detected through a test statistic based on the Galileo-GPS time offset (GGTO) parameter broadcast in the Galileo navigation message.

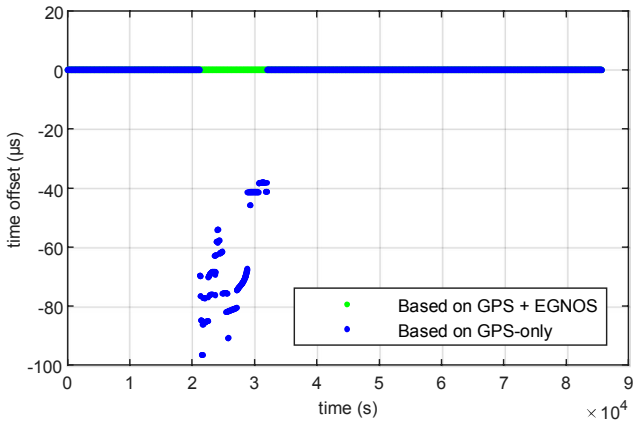

Fig. 9. Time offset of the GPS and GPS–EGNOS solution during a simulated single-satellite fault occurring between 21600 and 32400 s.

For two UTC(k) clock bias estimates $\hat{t}_i$ obtained from systems $i = 1, 2$, and having standard deviations $\hat{\sigma}_i$, the difference of the clock biases follows a standard distribution with mean equal to the difference of the two associated UTC(k) scales and standard deviation equal to $\hat{\sigma}_{1-2} = \sqrt{2\hat{\sigma}_{CAL}^2 + \hat{\sigma}_1^2 + \hat{\sigma}_2^2}$ where σ_{CAL} is the receiver hardware delay calibration uncertainty for one signal. The time solutions of the two systems are compared with a two-tailed test as follows:

$$\left|\hat{t}_1 - \hat{t}_2\right| < \hat{\sigma}_{1-2}\ invN(1 - p_F/2) \tag{5}$$

where $invN$ is the inverse cumulative density function of the standard normal distribution and p_F is a predetermined probability of false alarm chosen here as 10^{-5}. When using Galileo and GPS, the cross-check can be done directly on the Galileo time scale (GST) instead of UTC by applying the GGTO. This brings added benefits in that the GGTO has a much smaller variance than the UTC parameters, enabling better detection performance. Furthermore, testing in both UTC and GST will detect errors in the broadcast parameters.

Fig. 10 shows in blue the left-hand side of (5), the difference between GST based on the Galileo solution and the GPS-based solution converted to GST by applying the broadcast GGTO. The test threshold, the right-hand side of (5), is shown in red. The simulated navigation data error is clearly seen as a jump in the test statistic between hours 15 and 18, when the test statistic crosses the threshold. The unmitigated timing solution, shown in Fig. 11, displays a large error in excess of 100 μs, while if holdover was applied as a response to the GGTO-based fault detection, the navigation data error would be mitigated.

Using only two constellations, it cannot be determined which constellation is the faulty one; nevertheless, it allows the detection of a loss of integrity. Adding a third constellation would enable fault exclusion and continuing GNSS operation in this fault scenario.

C. Multipath

Fig. 12 shows the effect of multipath on MTIE under different multipath conditions. It can be observed that degradation in MTIE is proportional to the magnitude of the multipath

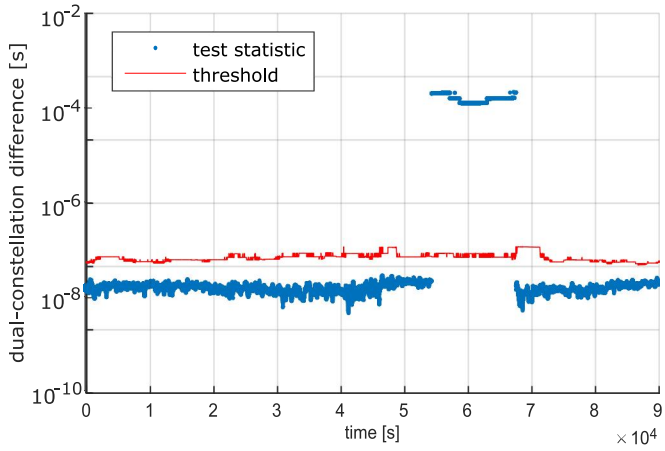

Fig. 10. Dual-constellation cross-check detection statistic (blue) and test threshold (red) during the simulated constellation-wide timing fault scenario.

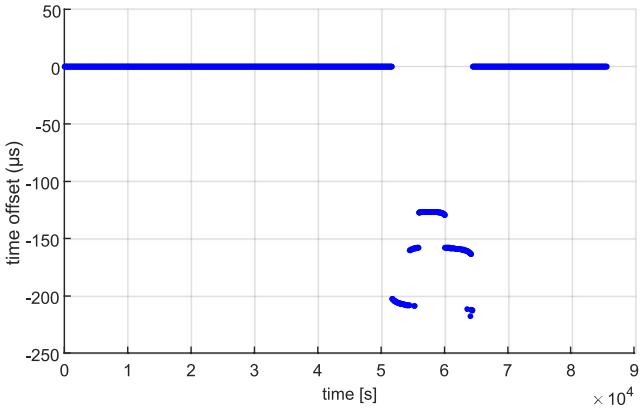

Fig. 11. Time offset of the GNSS solution during a simulated constellation-wide timing fault occurring between 14 h and 18 h.

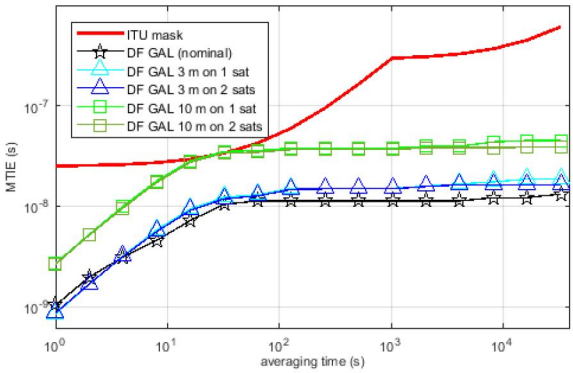

Fig. 12. MTIE for dual-frequency Galileo in the presence of different multipath scenarios. The degradation is directly proportional to the magnitude of the multipath error and exceeds the ITU mask when it is about 10 m.

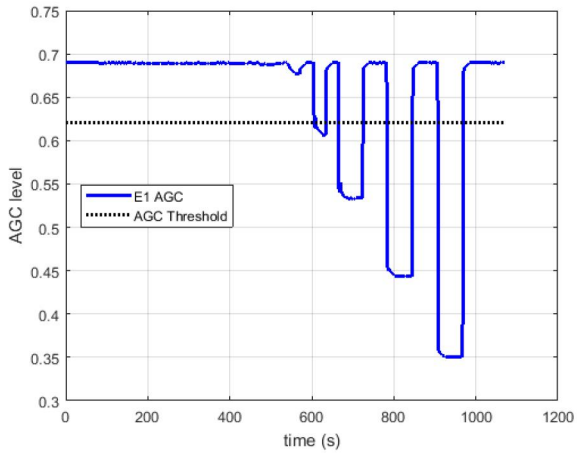

Fig. 13. Automatic gain control (AGC) values during jamming on E1. Short periods of jamming with increasing power are alternated with periods of no jamming, starting at 500 s. Jamming is detected when the AGC level falls below the threshold.

error. An error of 3 m on one or two satellites does not cause a breach of the ITU recommended MTIE limit. Only in the presence of 10 m multipath on two satellites, the MTIE exceeds the limit. The effect on TDEV, however, was very minor and is not shown here. Note that the total number of satellites used in the timing solution also has an influence on the degrading effect of the multipath error. Nevertheless, this scenario helps to demonstrate the efficacy of MTIE as a metric to study the effect of multipath on the timing solution.

D. Radio frequency interference

The following results are intended to test the timing performance under RF interference, and ways to mitigate that threat.

1) AGC and C/N_0 monitoring: The first part of the test evaluates methods of detecting interference by monitoring the receiver's AGC and C/N_0 values, when interference from a GNSS jammer is introduced, as illustrated in the test setup in Fig. 1. The AGC results with jamming on the E1 band are shown in Fig. 13. The effect of jamming is apparent in the blue curve, which shows the AGC on the E1 band. The corresponding situation can be seen in Fig. 14, where the jamming is on the E5 band. In both tests, the jammer is turned on at approximately 500 s, and alternated on and off while gradually increasing power. The AGC is very responsive to turning the jamming on and off.

In order to demonstrate a simple interference detection algorithm, the dotted black line represents a threshold at 90% mean AGC value in nominal conditions. An interference event is detected when the AGC level falls below this threshold. In the E1 jamming test, jamming is detected on E1 when jamming-to-signal ratio (J/S) exceeds 30 dB, and in the E5 jamming test, when J/S exceeds 60 dB. This difference can be attributed to the wider bandwidth of the Galileo E5 signal, which strengthens its anti-interference capability. These results demonstrate that AGC monitoring can be a suitable indicator for the presence of RF interference in the vicinity of GNSS-based timing receivers.

Fig. 15 shows the results of C/N_0 monitoring in the E1 jamming test as a method of interference detection. The curves represent the instantaneous C/N_0 for four Galileo satellites (identified by PRN number) under a condition of jamming on the E1 band. The dashed red curve shows the average C/N_0, which is compared to the threshold shown by the black line

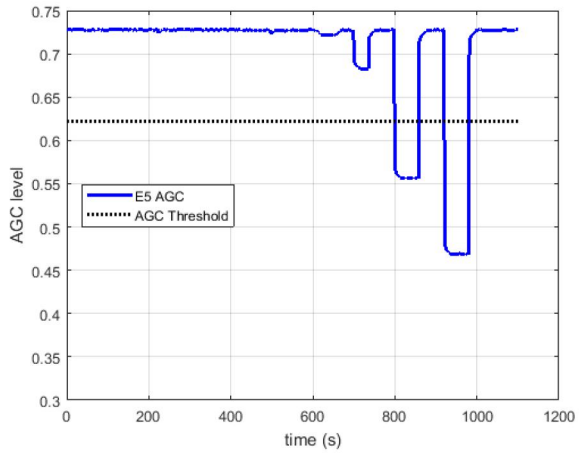

Fig. 14. Automatic gain control values during jamming on E5. Short periods of jamming with increasing power are alternated with periods of no jamming, starting at 500 s. Jamming is detected when the AGC level falls below the threshold.

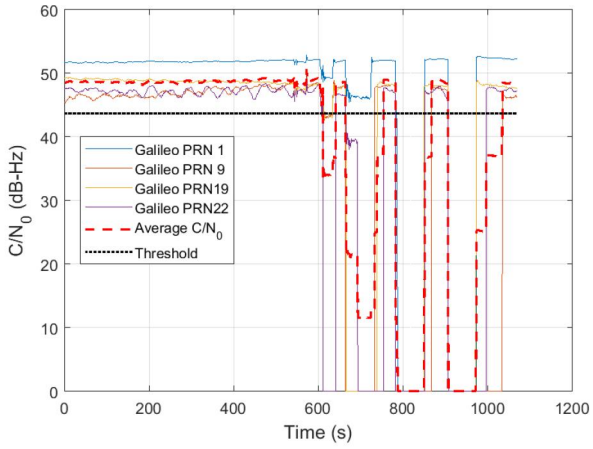

Fig. 15. E1 carrier-to-noise density ratio (C/N_0) values for four Galileo satellites during periodic jamming with increasing power on E1. Jamming is detected when the average C/N_0 falls below the threshold.

to detect the presence of jamming. This detection algorithm is not expected to be an optimal one; a detailed study of methods can be found, for instance, in [38]. The aim is to show that C/N_0 can also be used as a metric to determine the presence of RF interference in timing receivers.

2) Holdover: The effects of interference over a time span of 24 hours are presented in the following test, where artificial gaps were introduced in the recorded data set in order to simulate interference. 16 gaps of 1000 s length were introduced at regular intervals. This duration was chosen because it was expected to be long enough for the clock drift to accumulate. Fig. 16 shows the response of the time solution output, again as the difference from the recorded reference clock. During the GNSS gaps, the receiver enters holdover mode and the offset increases until GNSS is restored. Note that this is a hypothetical scenario as under real-world conditions the interference power would rarely be strong enough instantaneously

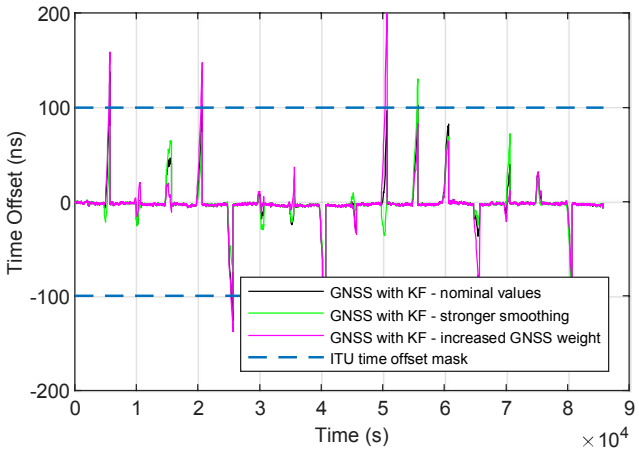

Fig. 16. Time offset between GNSS time and UTC for different KF realizations in holdover, with periodic artificial gaps in GNSS availability.

to cause a complete outage in the receiver but rather increase gradually. This would require the holdover to initiate from a more degraded signal condition than that considered here.

Three different holdover Kalman filters were evaluated, with three sets of design values based on the noise properties of the LO via tuning parameters as proposed in [39]. The state transition covariance noise matrix in this filter is determined based on so-called h-parameters derived from the Allan deviation curve of the LO. In this study, we compare three different tunings of the filter: the nominal one derived from the Allan deviation, a variant where the h-parameters were amplified by a factor of 100 to increase the weight of GNSS updates, and another variant where the h-parameters were scaled down by a factor of $1/100$ to apply a stronger smoothing, essentially down-weighting the GNSS measurements.The nominal condition gives relatively equal weight to both options. The dashed lines on the figure show the ITU recommended limits on maximum time offset.

The MTIE values are dominated by the jumps at the end of each holdover period. This is because MTIE is computed as the maximum time error variation within a certain interval, hence being sensitive to any sudden discrepancies in the timing solution due to artificial outliers arbitrarily dispersed in the experiments. While the absolute error accrued during holdover depends on the stability of the oscillator, this test demonstrates that the maximum time error caused by a GNSS outage depends strongly on the initial conditions at the start of the outage. The variance of outcomes is largest (23.4^2 ns) when the KF gives more weight on the last GNSS observables. Stronger smoothing produces a slightly smaller error variance (17.5^2 ns) than the nominal case (19.5^2 ns). However, the difference between them is quite small.

3) Dual-frequency: In order to illustrate the effect of dual-frequency GNSS timing operation as a mitigation technique against first-order ionospheric errors, which typically account for more than 99 % of the total ionospheric effect [40]. Fig. 17 shows the time offset of the SF and DF Galileo solutions during the simulated ionospheric threat. The SF solution, which uses the Galileo broadcast ionospheric corrections, is

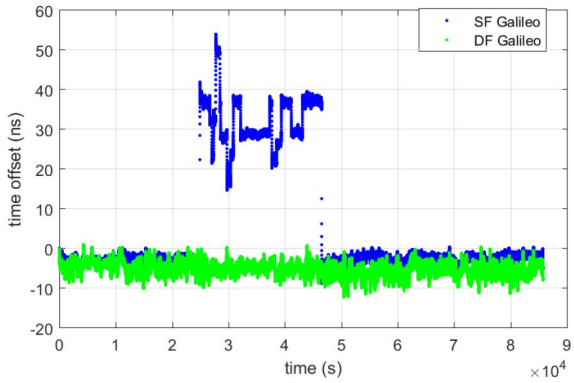

Fig. 17. Single- and dual-frequency Galileo time offset in the presence of ionospheric disturbance occurring between 25200 and 46800 s.

adversely affected, while the DF solution maintains nominal behavior and is unaffected by the ionospheric error. Because the first-order ionospheric errors are frequency dependent, they are compensated by the use of the DF ionosphere-free observation combination in the DF solution. Note that due to the currently low number of GPS satellites which provide dual-frequency capability on L1 and L5, it is expected that DF GPS-based solution may not provide significant benefits over single-frequency operation. This situation is expected to improve as more GPS satellites offer L1 and L5 signals simultaneously.

In order to test the benefit that multi-frequency GNSS receivers have against interference, we propose a dual-frequency Galileo timing receiver that automatically falls back to SF operation if one of the frequency bands becomes unavailable. To simulate interference, artificial gaps were introduced into the E1 observations at 6 time points, of 3600 s length each, at times between 1×10^4 and 6×10^4 s. The gaps in E1 observations render the dual-frequency solution unavailable. Fig. 18 shows the GNSS-UTC time offset when, in order to preserve the continuity of timing, the receiver falls back to single-frequency E5 solution during outages in E1.

Compared to the nominal DF case, the KPIs are degraded by the SF fallback, but they remain within the defined limits, as shown in Figs. 19 and 20. Most notably, the continuity of the timing service is preserved when otherwise service would be interrupted. This result demonstrates how DF GNSS can help to improve resilience against RF interference on part of the GNSS band through frequency diversity.

E. Signal spoofing

Fig. 21 shows how the GNSS time solutions behave under meaconing-type spoofing. Initially, the solutions are based on the authentic GNSS signals, with little differences. As the spoofer power is increased after 500 s, the timing solutions begin to deviate. SF Galileo maintains best continuity at the start of the spoofing, between 500 s and 1200 s. However, DF Galileo deviates wildly, suggesting some differences in the receiver's tracking loops in the different frequency bands in response to spoofing. On the other hand, the deviation can be explained by summing of the offset in the DF combination.

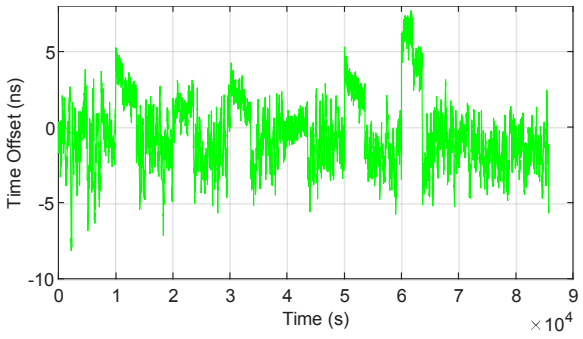

Fig. 18. Time offset between GNSS time and UTC. Nominal dual-frequency Galileo is interrupted by six 1-hour gaps. Gaps in dual-frequency Galileo are bridged by fallback to single frequency.

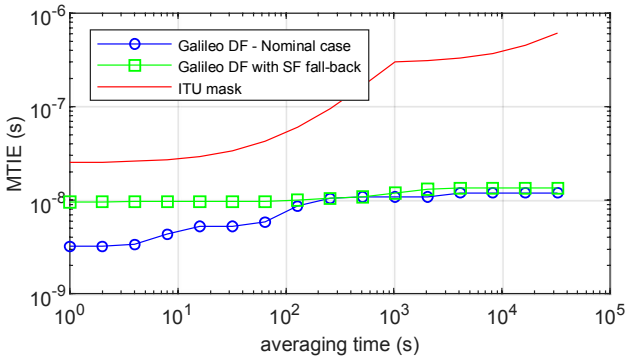

Fig. 19. Comparison of MTIE between dual-frequency Galileo and dual-frequency Galileo with single-frequency fallback. Although MTIE degrades due to the fallback option, it still remains within the ITU recommendation.

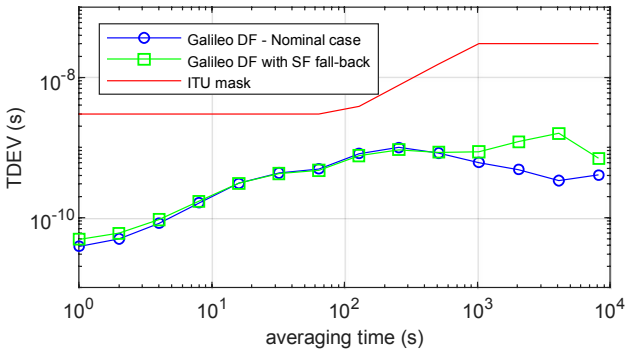

Fig. 20. Comparison of TDEV between dual-frequency Galileo and dual-frequency Galileo with single-frequency fallback.

At the instant when the spoofing to signal ratio exceeds 0 dB (spoofing power is greater than signal power), all timing solutions shift to about 90 ns offset from the true time. This offset corresponds to the time delay in the spoofing signal generation setup. From this moment on, the receiver is no longer tracking the authentic signals and the timing solutions are computed based on the spoofed signals.

Fig. 22 shows the variations of the AGC output values in response to the meaconing test. The E1 AGC is shown by the blue curve and the E5 AGC by the red curve. A predetermined threshold is set at 90% of the mean value in nominal conditions. If an AGC level falls below the threshold

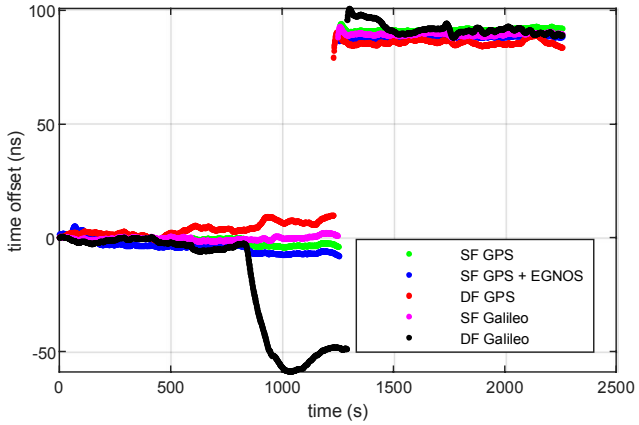

Fig. 21. Time offset between GNSS time and UTC during meaconing. In this scenario the meaconing signals overcome the authentic signals after 1200 s causing the abrupt shift in the timing solution.

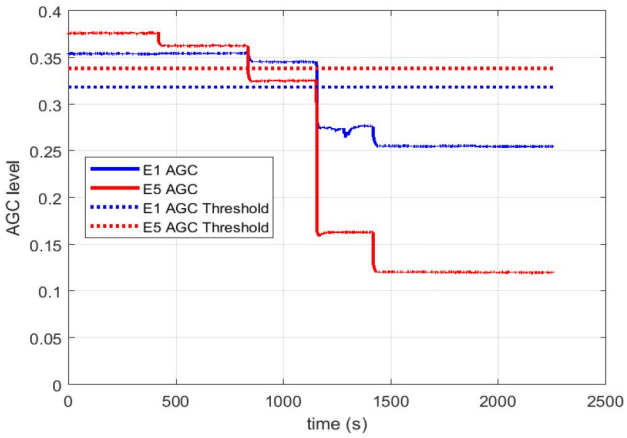

Fig. 22. AGC gain during meaconing. Presence of meaconing is detected when the AGC levels for the individual frequency bands fall below their respective thresholds.

(dotted lines), a detection is flagged. This occurs at a spoofing-to-signal ratio of approximately 0 dB for E1 band and –10 dB for E5 band. This difference between bands indicates that more spoofing signal energy enters the E5 band processing chain, which may explain the earlier deviation of the DF Galileo solution. The AGC drops to lower amplifications during the spoofing test because of the increased total received power when receiving both the spoofing signal and the authentic signal.

Fig. 23 shows C/N_0 measurements for Galileo E1 of three satellites and their average value. The C/N_0 values show some variations in response to the spoofing, but monitoring their average value alone does not seem to provide a reliable detection metric. For example, C/N_0 does not correlate with the increasing spoofing power, and shows only a momentary spike when the spoofing signal overcomes the authentic one. Conversely, the AGC value is correlated with the spoofing power. From these results we observe that AGC is a more reliable metric for spoofing detection, even though as most receivers provide only the C/N_0 as an observable discarding this metric is not advisable.

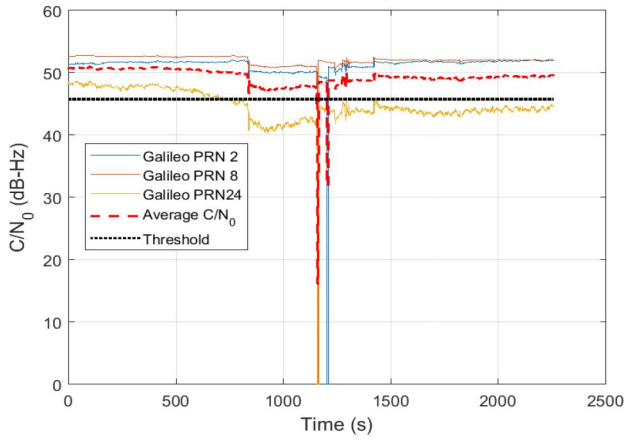

Fig. 23. E1 C/N_0 for three Galileo satellites during meaconing. Presence of meaconing is detected when the average C/N_0 falls below the threshold.

VI. Conclusions

We have studied timing computation based on GPS, Galileo, and EGNOS, and evaluated them based on their performance and robustness against various threat scenarios related to specific vulnerabilities in GNSS-based timing. We identified a number of robustness concepts, tested them with the aim to mitigate the threats, and analyzed their effectiveness against corresponding threats:

- RF Interference: A simple meaconing-type spoofing attack is able to hijack a simple timing solution, when the spoofing to signal power ratio exceeds 1. AGC and C/N_0 monitoring were demonstrated as options for jamming and spoofing detection. A comparison of Kalman filters during a simulated holdover operation suggests that stronger smoothing (achieved by filter tuning) leads to less accumulated error during holdover. The DF fallback strategy provides protection against RFI, with some degradation in stability.
- Navigation message errors: It is assumed that EGNOS integrity messaging helps to successfully discard faulty satellites from the timing solution. Based on this it was shown that using EGNOS in the timing receiver configuration helps in mitigating the effect on the time solution of navigation message errors in some satellites A dual-constellation cross-check algorithm using the GGTO parameter can detect a constellation-wide error affecting multiple satellites.
- Multipath: In addition to supporting the well-established conclusion that the degradation in the timing performance is proportional to the magnitude of the multipath error, this test case also demonstrated that increasing the multipath error on the affected satellite resulted in a larger adverse effect as compared to simulating the original multipath on a higher number of satellites.
- Ionosphere: First-order ionospheric effects can be miti-

gated by using dual-frequency GNSS, improving long-term time solution stability at the cost of increased short-term noise.

Therefore, a receiver computing EGNSS-enabled timing solution and equipped with the proposed robustness features satisfies the recommendations of the ITU for PRTCs under the threat conditions considered here. In other cases it is possible to detect the presence of the threat by observing certain receiver performance metrics. While single-frequency GPS provides better timing stability in terms of MTIE and TDEV, simulations show that Galileo has a slight advantage when satellite numbers are equal.

While it can be acknowledged that this is not an exhaustive list of threat scenarios, this is the first comprehensive overview of the overall performance and robustness of GNSS timing with respect to some of the most commonly identified threats. These aspects have not been studied before for Galileo and EGNOS in this level of detail (or for GNSS in general as a whole).

ACKNOWLEDGMENT

The authors acknowledge the assistance from VTT MIKES Metrology for use of their precise timing facility in Espoo, Finland, and Dr. Daniele Borio from the Joint Research Centre of the European Commission for valuable technical advice.

REFERENCES

[1] G. J. Geier, T. M. King, H. L. Kennedy, R. D. Thomas, and B. R. McNamara, "Prediction of the time accuracy and integrity of GPS timing," in *Proceedings of the 1995 IEEE International Frequency Control Symposium (49th Annual Symposium)*, 1995, pp. 266–274.

[2] L. Gasparini, O. Zadedyurina, G. Fontana, D. Macii, A. Boni, and Y. Ofek, "A digital circuit for jitter reduction of GPS-disciplined 1-pps synchronization signals," in *2007 IEEE International Workshop on Advanced Methods for Uncertainty Estimation in Measurement*, 2007, pp. 84–88.

[3] M. A. Lombardi, L. M. Nelson, A. N. Novick, and V. S. Zhang, "Time and frequency measurements using the Global Positioning System," *Cal Lab: International Journal of Metrology*, vol. 8, no. 3, pp. 26–33, 2001.

[4] M. A. Lombardi, "The use of GPS disciplined oscillators as primary frequency standards for calibration and metrology laboratories," *NCSLI Measure*, vol. 3, no. 3, pp. 56–65, 2008.

[5] S. Bittl, A. A. Gonzalez, M. Myrtus, H. Beckmann, S. Sailer, and B. Eissfeller, "Emerging attacks on VANET security based on GPS time spoofing," in *2015 IEEE Conference on Communications and Network Security (CNS)*. IEEE, 2015, pp. 344–352. [Online]. Available: http://dx.doi.org/10.1109/CNS.2015.7346845

[6] Z. Zhang, S. Gong, A. D. Dimitrovski, and H. Li, "Time synchronization attack in smart grid: Impact and analysis," *IEEE Transactions on Smart Grid*, vol. 4, no. 1, pp. 87–98, 2013. [Online]. Available: http://dx.doi.org/10.1109/TSG.2012.2227342

[7] X. Jiang, J. Zhang, B. J. Harding, J. J. Makela, and A. D. Dominguez-Garcia, "Spoofing GPS receiver clock offset of phasor measurement units," *IEEE Transactions on Power Systems*, vol. 28, no. 3, pp. 3253–3262, 2013.

[8] L. Heng, D. Chou, and G. X. Gao, "Reliable GPS-based timing for power systems," *Inside GNSS*, vol. November/December, pp. 38–45, 2014.

[9] O. Garitselov and D. Sohn, "Metamodel-assisted disciplining algorithm for detecting spoofed GNSS time signals," in *Proceedings of the 46th Annual Precise Time and Time Interval Systems and Applications Meeting*, Dec. 2014, pp. 221–227.

[10] Y. Wang and J. P. Hespanha, "Distributed estimation of power system oscillation modes under attacks on GPS clocks," *IEEE Transactions on Instrumentation and Measurement*, vol. 67, no. 7, pp. 1626–1637, 2018.

[11] A. Mujunen, J. Aatrokoski, M. Tornikoski, and J. Tammi, *GPS Time Disruptions on 26-Jan-2016*, ser. Aalto University publication series SCIENCE + TECHNOLOGY. Aalto University, 2016, vol. 2/2016.

[12] N. C. Lombardi, M. A. and W. J. Walsh, "The role of LORAN timing in telecommunications," in *Proceedings of Radio Technical Commission for Maritime Services Conference (RTCM)*, 2006.

[13] G. Johnson and P. Swaszek, *Accseas: Feasibility Study of R-Mode using MF DGPS Transmissions*, 2014. [Online]. Available: http://www.accseas.eu/content/download/4675/40172/file/R-Mode_Study_MF-Beacon_final_20140311.pdf

[14] J. A. Davis and B. Rougeaux, "The development of a computer model of a GPS disciplined oscillator to aid error budget determination," in *Proceedings of the 1999 Joint Meeting of the European Frequency and Time Forum and the IEEE International Frequency Control Symposium (Cat. No.99CH36313)*, vol. 1, 1999, pp. 291–295.

[15] Y. Chen, D. Reale, J. Dickens, S. Holt, J. Mankowski, and M. Kristiansen, "Phased array pulsed ring-down source synchronization with a GPS based timing system," *IEEE Transactions on Dielectrics and Electrical Insulation*, vol. 18, no. 4, pp. 1071–1078, 2011.

[16] X. Niu, K. Yan, T. Zhang, Q. Zhang, H. Zhang, and J. Liu, "Quality evaluation of the pulse per second (PPS) signals from commercial GNSS receivers," *GPS Solutions*, vol. 19, no. 1, pp. 141–150, 2015. [Online]. Available: http://dx.doi.org/10.1007/s10291-014-0375-7

[17] D. Itagaki, K. Ohashi, I. Shuto, and H. Ito, "Field experience and assessment of GPS signal receiving and distribution system for synchronizing power system protection, control and monitoring," in *2006 IEEE Power India Conference*, 2006.

[18] P. Vyskocil and J. Sebesta, "Relative timing characteristics of GPS timing modules for time synchronization application," in *2009 International Workshop on Satellite and Space Communications*, 2009, pp. 230–234.

[19] X. Zhao, D. M. Laverty, A. McKernan, D. J. Morrow, K. McLaughlin, and S. Sezer, "GPS-disciplined analog-to-digital converter for phasor measurement applications," *IEEE Transactions on Instrumentation and Measurement*, vol. 66, no. 9, pp. 2349–2357, 2017.

[20] W. Lewandowski, G. Petit, and C. Thomas, "Precision and accuracy of GPS time transfer," *IEEE Transactions on Instrumentation and Measurement*, vol. 42, no. 2, pp. 474–479, Apr. 1993.

[21] S. H. Yang, Y. K. Lee, Y. J. Heo, S. W. Lee, and C. B. Lee, "Comparison of time transfer using GPS carrier phase and multichannel two-way data in East Asia," *IEEE Transactions on Instrumentation and Measurement*, vol. 56, no. 2, pp. 664–668, Apr. 2007.

[22] A. Bauch and P. Whibberley, "Reliable time from GNSS signals," *Inside GNSS*, vol. March/April, pp. 38–45, 2017.

[23] P. Defraigne, "Multi-GNSS time and frequency transfer," in *Journées 2013 "Systèmes de référence spatio-temporels"*, 2014, pp. 109–114.

[24] P. Defraigne, W. Aerts, G. Cerretto, E. Cantoni, and J. M. Sleewaegen, "Calibration of Galileo signals for time metrology," *IEEE Transactions on Ultrasonics, Ferroelectrics, and Frequency Control*, vol. 61, no. 12, pp. 1967–1975, 2014.

[25] D. S. De Lorenzo, S. C. Lo, J. Seo, Y.-H. Chen, and P. K. Enge, "The WAAS/L5 signal for robust time transfer: Adaptive beamsteering antennas for satellite time synchronization," in *Proceedings of the 23rd International Technical Meeting of the Satellite Division of the Institute of Navigation*, 2010, pp. 2106–2116.

[26] European GNSS Agency, *EGNOS Safety of Life (SoL) Service Definition Document, issue 3.0*, 2015. [Online]. Available: http://dx.doi.org/10.2878/851094

[27] European Union, *Galileo Open Service Signal-In-Space Interface Control Document, issue 1.2*, 2015. [Online]. Available: https://www.gsc-europa.eu/system/files/galileo_documents/Galileo-OS-SIS-ICD.pdf

[28] S. Söderholm, M. Z. H. Bhuiyan, S. Thombre, L. Ruotsalainen, and H. Kuusniemi, "A multi-GNSS software-defined receiver: design, implementation, and performance benefits," *Annals of Telecommunications*, vol. 71, no. 7-8, pp. 399–410, Aug. 2016. [Online]. Available: http://dx.doi.org/10.1007/s12243-016-0518-7

[29] European GNSS Agency, "Report on time & synchronisation user needs and requirements, issue 1.0," Oct. 2018.

[30] M. Kirkko-Jaakkola, S. Thombre, S. Honkala, S. Söderholm, S. Kaasalainen, H. Kuusniemi, H. Zelle, H. Veerman, and A. Wallin, "Evaluating the robustness of EGNSS based timing services," in *Proceedings of the European navigation Conference (ENC 2017)*, 2017.

[31] M. Kirkko-Jaakkola, S. Thombre, S. Honkala, S. Söderholm, S. Kaasalainen, H. Kuusniemi, H. Zelle, H. Veerman, A. Wallin, K. A. Aarmo, and J. P. Boyero, "Receiver-level robustness concepts for EGNSS timing services," in *Proceedings of the 30th International Technical Meeting of The Satellite Division of the Institute of Navigation (ION GNSS+ 2017)*, 2017, pp. 3353 – 3367.

[32] M. A. Lombardi, "Time measurement," in *Measurement, Instrumentation, and Sensors Handbook, Second Edition: Electromagnetic, Optical,*

Radiation, Chemical, and Biomedical Measurement, J. G. Webster and H. Eren, Eds. CRC Press, 2014.
[33] "Timing characteristics of primary reference clocks, International Telecommunication Union recommendation ITU-T G.811, Amendment 1," Apr. 2016. [Online]. Available: https://www.itu.int/rec/T-REC-G.811/en
[34] W. Riley and D. A. Howe, "Handbook of frequency stability analysis," *Special Publication (NIST SP) - 1065*, 2008. [Online]. Available: https://www.nist.gov/publications/handbook-frequency-stability-analysis
[35] Novatel Inc., "ProPak6 product sheet D18297 Rev. 7," Nov. 2015. [Online]. Available: https://www.novatel.com/assets/Documents/Papers/ProPak6-PS-D18297.pdf
[36] KVG Quartz Crystal Technology GmbH, "T-9601F product sheet," Neckarbischofsheim, Germany, Apr. 2005.
[37] Keysight Technologies, "53200 Series RF/Universal Frequency Counters/Timers - data sheet," Apr. 2016. [Online]. Available: https://literature.cdn.keysight.com/litweb/pdf/5990-6283EN.pdf?id=1942617
[38] D. Borio, F. Dovis, H. Kuusniemi, and L. L. Presti, "Impact and detection of GNSS jammers on consumer grade satellite navigation receivers," *Proceedings of the IEEE*, vol. 104, no. 6, pp. 1233–1245, June 2016.
[39] A. J. Van Dierendonck, J. B. McGraw, and R. G. Brown, "Relationship between Allan variances and Kalman filter parameters," *Proc. 16 Precise Time and Time Interval Application and Planning Meeting*, p. 22, Nov. 1984.
[40] H. A. M. Z. G. Elmas, M. Aquino and J. F. G. Monico, "Higher order ionospheric effects in gnss positioning in the european region," *Ann. Geophys.*, vol. 29, pp. 1383–1399, 2011. [Online]. Available: https://www.ann-geophys.net/29/1383/2011/angeo-29-1383-2011.pdf

Salomon Honkala received the M.Sc.(Tech.) degree in electrical engineering from Aalto University, Espoo, Finland in 2016. He is a Research Scientist in the Satellite and Radio Navigation research group at the Department of Navigation and Positioning at the Finnish Geospatial Research Institute (FGI), Kirkkonummi, Finland, and a Ph.D. candidate at Tampere University of Technology, Finland. His research interests include GNSS vulnerabilities, software GNSS receiver design, interference mitigation, GNSS timing robustness, precise positioning, and Arctic navigation.

Sarang Thombre earned the D.Sc.(Tech) degree in 2014 from Tampere University of Technology. He is a Research Manager leading the Satellite and Radio Navigation research group at the Department of Navigation and Positioning of FGI. He is an External Project Reviewer for the European GNSS Agency within the Horizon 2020 Galileo programme, and a member of the Board of the Nordic Institute of Navigation. His research interests are in multi-GNSS, multi-frequency, and Timing receiver implementation and performance validation, interference detection, and autonomous navigation solutions for road and marine vehicles.

Martti Kirkko-Jaakkola received the M.Sc. and D.Sc. (Tech.) degrees from Tampere University of Technology, in 2008 and 2013, respectively. From 2006 till 2013 he worked with the Department of Pervasive Computing, Tampere University of Technology, including research visits to the Technical University of Munich, Germany, and the European Space Research and Technology Centre, The Netherlands. Currently, he works as a Research Manager at the Finnish Geospatial Research Institute (FGI) in Kirkkonummi, Finland, where he leads the Sensors and Indoor Navigation research group. His research interests include low-cost precise satellite positioning, microelectromechanical inertial sensors, and GNSS-based time transfer.

Hein Zelle earned the Ph.D. degree in 2005 in physical oceanography from the university of Utrecht, the Netherlands. He has worked on numerical weather modelling, air quality modelling and their application in services. Since 2012 he has specialized in satellite navigation (GNSS). At NLR he is a senior R&D engineer, leading the GNSS R&D activities. Research topics focus on ionospheric monitoring and corrections, tropospheric corrections, robust GNSS receivers and antennas, GNSS timing applications, quality and performance monitoring and Galileo 2nd generation evolutions.

Henk Veerman received the M.Sc. degree in experimental physics at the University of Amsterdam. Now as a senior scientist at NLR, he works on novel technologies for application in aeronautics, with a focus on GNSS, data link communication and optical measurement techniques. He has been involved in GNSS research since 2000, investigating EGNOS and Galileo performances and prospects for aeronautical application, specializing on GNSS integrity studies, modeling signal atmospheric propagation, RF interference and working on GBAS for Cat II / III application.

Anders E. Wallin obtained the Ph.D. degree in physics from the University of Helsinki, Finland, in 2011. Since 2012 he is with VTT MIKES Metrology, Espoo, Finland. Current reasearch interests include time and frequency metrology, including single-ion optical clocks, time transfer systems, and high-accuracy time distribution/measurement techniques.

Erik F. Dierikx Erik F. Dierikx was born in Aardenburg, The Netherlands, in 1972. In 1995, he received the M.Sc. degree in electrical engineering from the University of technology, Eindhoven, The Netherlands, working on "Low frequency noise in quantum well lasers".

In 1995, he joined the Electricity and Magnetism section at VSL (the Dutch metrology institute), Delft, The Netherlands and specialized in low-frequency impedance measurements. From 2006, he became involved in the Time & Frequency section at VSL, contributing to a delay calibration system for a two-way satellite time and frequency transfer station. From 2012, he has been mainly working on time and frequency transfer through optical fibers. Currently, he is technically responsible for the activities in the Time & Frequency section at VSL.

Sanna Kaasalainen received the Ph.D. degree in astronomy from the University of Helsinki in 2003. She is currently a professor and director of the Department of navigation and positioning at the Finnish Geospatial Research Institute, and a docent (Adjunct Prof.) in Aalto University School of Engineering. Her research interests include optical sensors in positioning and environmental studies, and their integration in improved situational awareness and smart realtime sensing methods.

Stefan Söderholm received the M.Sc. degree from Åbo Akademi University, Turku, Finland, department of Experimental Physics, in 1991 and the Licentiate degree from University of Turku, Department of Applied Physics, in 1996.

He is currently working as the GNSS Team Leader at HERE Technologies where he is heading the companies work on improving GNSS accuracy and reliability. This includes algorithm development and product specifications within the technology areas of Precise Point Positioning, anti-jamming and anti-spoofing. Stefan is also a doctoral candidate at Tampere University of Technology, and his research interests cover multi-GNSS receiver design, BOC signal processing, GNSS spoofing and interference detection and PPP/RTK methods.

Heidi Kuusniemi is research professor in satellite navigation at the Finnish Geospatial Research Institute of the National Land Survey of Finland. She is also the director of the multi-disciplinary research platform Digital Economy at the University of Vaasa in Finland. She has worked in research and development within positioning technologies for over 18 years. She is an Adjunct Professor in satellite navigation and positioning technologies at Tampere University and Aalto University in Finland. She is also the president of the Nordic Institute of Navigation. She serves as a member of the council of natural sciences and technology at the Academy of Finland. Her research interests include GNSS reliability monitoring, GNSS interference detection and mitigation, self-contained sensors, indoor positioning, IoT, and the digital economy.